

Original

A micro-CT study of the greater palatine foramen in human skulls

Mia-Michaela Beetge¹⁾, Vladimir S. Todorovic^{1,2)}, Anna Oettlé³⁾,
Jakobus Hoffman⁴⁾, and Andre W. van Zyl¹⁾

¹⁾Department of Periodontics and Oral Medicine, School of Dentistry, University of Pretoria, Pretoria, South Africa

²⁾School of Dental Medicine, University of Belgrade, Beograd, Serbia

³⁾Department of Anatomy, Faculty of Health Sciences, University of Pretoria, Pretoria, South Africa

⁴⁾South African Nuclear Energy Corporation, Pretoria, South Africa

(Received November 11, 2016; Accepted February 9, 2017)

Abstract: The greater palatine foramen (GPF) is an important anatomical landmark and has substantial clinical relevance in dental surgery. Knowledge of its precise location and dimensions is required for proper planning of surgical procedures involving the posterior maxilla. We used microfocus computed tomography to determine the location and dimensions of the GPF, and any sex and race variations in those measurements, in 77 human skulls scanned at the South African Nuclear Energy Corporation. Specialized software was used for three-dimensional rendering, segmentation, and visualization of the reconstructed volume data. GPF location ranged from adjacent to the first molar to distal of the third molar. The most common GPF location was near the third molar (66.7% of skulls), and the GPF was as close as 6.31 mm (mean distance 12.75 ± 3 mm). The mean GPF dimensions were 5.22 mm on the anterior-posterior axis and 2.81 mm on the lateral-medial axis. We noted no significant differences in relation to race, sex, or age in the sample. The GPF was adjacent or posterior to the third maxillary molar in most skulls.

Keywords: micro-CT; greater palatine foramen; anatomy; palate.

Introduction

The greater palatine foramen (GPF) is an important landmark in oral surgery. Block anesthesia of the greater palatine nerve (GPN) is a very common procedure in numerous dental interventions involving the posterior maxilla. Procedures that may involve the GPF include orthognathic surgery, closure of oroantral/nasal fistulas, removal of pathological tissue, harvesting of palatal soft tissue grafts, and extraction of maxillary posterior teeth (1-4). Harvesting of palatal masticatory mucosa for grafting procedures around natural teeth and dental implants is now almost routine in periodontal and implant surgery. However, these procedures are all performed close to, and thus may damage, vital anatomical structures, such as the greater palatine neurovascular complex (1,2,5,6). To avoid complications associated with vascular and nervous structures in the pterygopalatine fossa, practitioners must have a sound knowledge of the anatomy of this region.

The GPN is an important anatomical structure in the posterior maxilla. Within the pterygopalatine fossa the GPN originates from the maxillary nerve and emerges into the oral cavity through the GPF via the greater palatine canal (7,8). As the GPN exits the GPF, it progresses anteriorly within a well-defined groove between the hard palate and alveolar process, almost to the incisors, where it communicates with the nasopalatine nerve (2,3,9). The

Correspondence to Dr. Vladimir S. Todorovic, Department of Periodontics and Oral Medicine, School of Dentistry, University of Pretoria, PO Box 1266, Pretoria 0001, South Africa
Fax: +27-123-263-375 E-mail: todent@yahoo.com

J-STAGE Advance Publication: February 26, 2018

Color figures can be viewed in the online issue at J-STAGE.

doi.org/10.2334/josnusd.16-0783

DN/JST.JSTAGE/josnusd/16-0783

greater palatine artery and GPN constitute the neurovascular bundle that supplies the palatine and maxillary bones, as well as the palatal mucoperiosteum, glands, and gingiva. The GPN is found to be medial to the greater palatine artery and innervates the soft and hard tissues of the hard palate (4). While in the greater palatine canal, the GPN gives rise to posterior-inferior nasal branches. Anesthesia applied at this level affects the maxillary teeth, palatal soft tissues, and the skin of the mid-face, as well as the mucosa of the nasal cavity and maxillary sinuses (9). The lesser palatine nerves travel through the greater palatine canal and in approximately 50% of cases emerge through the lesser palatine foramina, giving branches to the uvula, tonsils, and soft palate (10). The lesser palatine foramina pierce the inferior surface of the pyramidal process of the palatine bone. These openings can be found behind the GPF, between the lower ends of the medial and lateral pterygoid plates (7,9).

Matsuda (11) first identified and described the location of the GPF, in 1927. Several later studies of the anatomy of GPF described its actual position in different populations (1-5,10,12-16). The variability in its location might be attributable to population differences in sutural growth between the maxillary and palatine bones or to different rates of growth after eruption of maxillary posterior teeth. Differences in the methods used in previous studies could also contribute to variation in the reported location of the GPF (2,3,5).

High-precision microfocus computed tomography (micro-CT) imaging is superior to conventional medical cone-beam computed tomography (CBCT). Although both imaging modalities are based on the same principle, spatial resolution is 1 to 3 μm for micro-CT and 300 μm for CBCT. To obtain a high-quality three-dimensional (3-D) virtual image at this high spatial resolution, the number of two-dimensional (2-D) projections (radiographs taken in 360° of the sample) required increases from 375 to 8,000. The resulting tomogram (3-D image) is of much higher quality than a CBCT image and allows for more accurate quantitative analysis (Hoffman JW, De Beer F. Characteristics of the micro-focus x-ray tomography facility (MIXRAD) at Necsa in South Africa. 18th World Conference on Nondestructive Testing, 2012).

We used micro-CT to determine the position of the GPF relative to maxillary molars and measure its dimensions in the South African population. To our knowledge, this is the first time micro-CT has been used for this purpose.

Materials and Methods

Ethics approval was obtained from the Research Ethics Committee of the Faculty of Health Sciences, University

Table 1 Demographic data for decedents from whom skulls were obtained

Race and sex	<i>n</i>	Average age (years)
Black men	20	46.7 (\pm 15.7)
Black women	20	40.6 (\pm 14.1)
White men	20	61.7 (\pm 15.0)
White women	17	67.1 (\pm 10.5)
Total	77	53.5 (\pm 17.5)

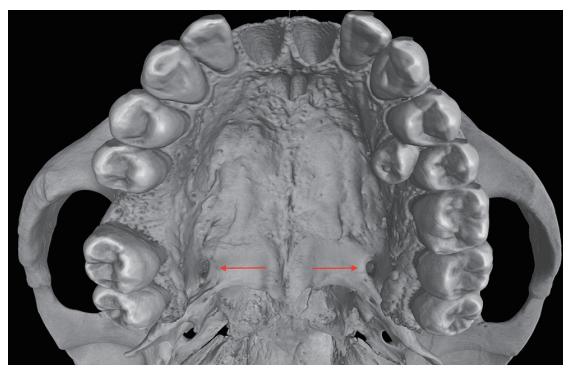


Fig. 1 Three-dimensional view of skull scanned with micro-CT; arrows indicate position of GPFs on inferior surface of hard palate.

of Pretoria, South Africa (No. 111/2013). The study sample consisted of 77 dry human skulls (Pretoria Bone Collection, University of Pretoria, South Africa) that represented two South African population subgroups and both sexes. The age at death of the decedents from whom the 77 specimens were obtained ranged from 22 to 90 years (mean age, 54 years). Completely edentulous maxillae were excluded. The race, sex, and mean age of the decedents are shown in Table 1.

The skulls were scanned with a micro-focus CT unit (Nikon XTH 225 ST, Nikon Metrology SARL, Lisses, France) at the Micro-Focus X-ray Tomography Facility (MIXRAD) of the South African Nuclear Energy Corporation (NECSA). The scans were performed at 100 kV and 100 μA , and the exposure time was 2000 milliseconds. The obtained resolution ranged between a voxel size of 105 and 112 μm . The volume files were imported into advanced volume rendering software (VGStudio MAX 2.2, Volume Graphics GmbH, Heidelberg, Germany) for 3-D rendering, segmentation, and visualization of the reconstructed volume data (Fig. 1). The software has interesting features, namely, a menu of analytical functions for quantitative analysis of virtual volume, so that distances in 3-D space can be measured by combining information provided by the 3-D image with axial, sagittal, and frontal views that show additional xy, yz, and xz slices, respectively. A virtual volume is defined by a specific number of voxels—the 3-D equivalent of 2-D

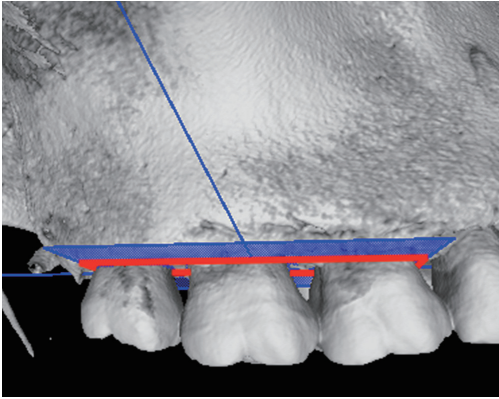


Fig. 2 Molar plane at level of alveolar crest (a micro-CT image).



Fig. 3 Individual plane created over a GPF (red outline).

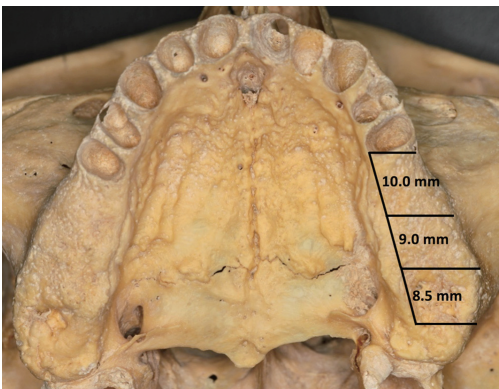


Fig. 4 Photograph showing average mesial-distal dimensions used in partially edentulous skulls.

pixels in a digital photograph. Each voxel indicates, but is not directly derived from, density. Therefore, the voxel value should be higher for compact bone than for porous cortical bone. Voxel values are displayed on a 16-bit scale and thus range from 0 to 65,535 (the highest density). All the present measurements were done simultaneously by two experienced specialists, in periodontics and oral medicine (professor and senior lecturer), according to a standardized protocol.

Measurements

Measurements taken in 3-D space on the reconstructed

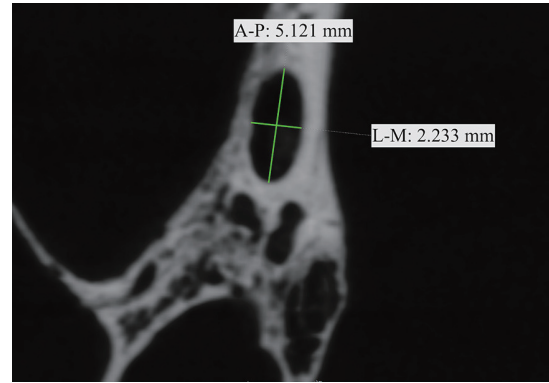


Fig. 5 Anterior-posterior and lateral-medial GPF dimensions (axial plane).

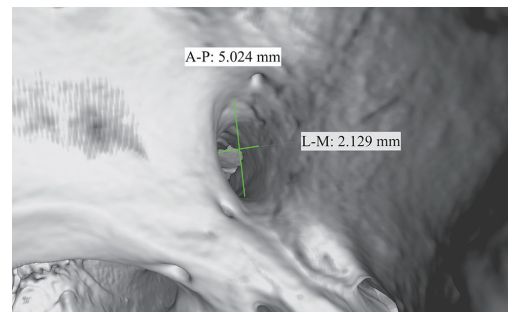


Fig. 6 GPF measurements viewed in 3-D.

images included the relative position of the anterior margin of the GPF, the distance between the GPF and a plane created at the alveolar crest (the molar plane), and the dimensions of the GPF. To establish a reproducible area from which the GPF could be observed, a molar plane (MP) was created at the alveolar crest of the first and third molar (or the approximate location if the individual was partially edentulous). Skull orientation was determined according to this set plane (Fig. 2). When GPF measurements were made, reference planes were created over each GPF (Fig. 3).

Location of the GPF

The location of the GPF was determined by assessing its anterior margin position relative to the maxillary molars. In samples without molar teeth, the location was approximated by subtracting the average mesiodistal widths of the crowns of the missing maxillary premolar and molar teeth (Fig. 4), as described by Nelson (Nelson SJ. Wheeler's dental anatomy, physiology and occlusion. Elsevier, 2014).

Distance between the GPF and MP

The MP was defined as the zero level from which the entire skull was oriented. From the zero level each sample was scrolled in a direction toward the point mark for the

Table 2 Distance from greater palatine foramen (GPF) to molar plane (MP) and GPF dimensions (mm)

Parameter	Subgroup	<i>n</i>	Right side		Left side	
			Mean (SD)	<i>P</i> value	Mean (SD)	<i>P</i> value
GPF-MP	Black men	20	13.17 (±2.91)	0.816	13.63 (±3.0)	0.116
	Black women	20	12.46 (±2.32)		13.15 (±2.60)	
	White men	20	12.86 (±3.31)		12.81 (±3.65)	
	White women	17	12.22 (±2.70)		11.35 (±3.22)	
	Total	77	12.70 (±2.80)		12.79 (±3.18)	
GPF (A-P)	Black men	20	5.43 (±1.11)	0.091	5.34 (±0.68)	0.067
	Black women	20	4.73 (±1.33)		4.62 (±0.81)	
	White men	20	5.60 (±0.70)		5.35 (±1.02)	
	White women	17	5.69 (±0.85)		5.00 (±1.07)	
	Total	77	5.35 (±1.08)		5.08 (±0.94)	
GPF (L-M)	Black men	20	3.05 (±0.44)	0.054	2.99 (±0.69)	0.061
	Black women	20	2.51 (±0.50)		2.29 (±0.43)	
	White men	20	2.95 (±0.56)		3.34 (±0.93)	
	White women	17	2.74 (±0.52)		2.58 (±0.54)	
	Total	77	2.81 (±0.54)		2.81 (±0.78)	

A-P: anterior-posterior; L-M: lateral-medial. *P* value (Kruskal-Wallis test).

anterior border of the GPF. Once the plane reached the point mark, the distance travelled (in mm) was recorded as the closest distance from the GPF to the alveolar crest.

Dimensions of the GPF

Because the skulls were previously oriented in relation to the MP, individual planes were created over each GPF in 3-D view to avoid bias related to the inappropriate reference plane when measuring GPF dimensions. Later, GPF dimensions were measured in 2-D view (axial plane), as follows: length—the anterior-posterior line from the point marker on the anterior border of the GPF to the most distal point of the GPF; width—the line perpendicular to the anterior-posterior line at the widest point of the GPF (Fig. 5). Measurements in 3-D view are shown in Fig. 6.

Statistical analysis

Data were analyzed for the group as a whole and also by sex and population group. The precision of the estimates of mean values was expressed as 95% confidence intervals. Data were recorded on an Excel spreadsheet, and descriptive (prevalence, mean, and standard deviation) and comparative analyses were performed in R by using the relevant function. The Kruskal-Wallis rank test was used for nonparametric tests of differences between groups. Statistical significance was set at $P < 0.05$.

Results

Table 2 shows the mean distances from the GPF to the MP and the dimensions of the GPF in the investigated groups. The anterior-posterior dimension (A-P) of the GPF ranged from 1.08 to 9.65 mm (mean: 5.35 ± 1.08 mm on the right side and 5.08 ± 0.94 mm on the left

side). The lateral-medial dimension (L-M) of the GPF ranged from 1.52 to 6.28 mm (mean: 2.81 ± 0.54 mm on the right side and 2.81 ± 0.78 on the left side). The average distance from the anterior margin of the GPF to the plane over the alveolar crest of maxillary molars was 12.70 ± 2.80 mm on the right side and 12.79 ± 3.18 mm on the left side.

The anterior margin of the GPF corresponded to the third molar in 66.7% of specimens and was posterior to the second molar in 83.5% of specimens. Linear measurements of the GPF did not show statistically significant sex or racial differences (Table 2). Table 2 shows GPF distribution by side, and Table 3 shows GPF location in relation to maxillary molar teeth.

Discussion

The GPF is located in an area of confluence of several anatomical structures and has substantial clinical relevance in oral and maxillofacial surgery, periodontal plastic surgery, and general dentistry. A literature search revealed no previous micro-CT studies of the GPF.

Most studies of the location and dimensions of the GPF used dry skulls (4,5,10,13-18) and cadavers (2,6,13). More-recent studies used medical CT and CBCT to evaluate the topography and structures within the palate (1,3,9,19,20). In European studies (3,14,15) the GPF was adjacent to third maxillary molars in 74.6% of cases and distal to third molars in 2.2% of cases. African studies (4,11) showed that the GPF was adjacent to third molars in 68.75% of cases and distal to third molars in 36.5% of cases. In studies that included Asians (2,13) the GPF was adjacent to third molars in 42.03% of cases and distal to third molars in 6.9% of cases. A high prevalence of third

Table 3 Location of GPF in relation to maxillary molar teeth

Category	Population group	Right foramen Average %	Left foramen Average %
First molar	Black men (<i>n</i> = 20)	2.1	1.8
	Black women (<i>n</i> = 20)	1.2	1.3
	White men (<i>n</i> = 20)	1.5	1.4
	White women (<i>n</i> = 17)	1.4	1.3
Second molar	Black men (<i>n</i> = 20)	19.1	16.9
	Black women (<i>n</i> = 20)	15.6	17.0
	White men (<i>n</i> = 20)	16.2	17.7
	White women (<i>n</i> = 17)	15	17.5
Third molar	Black men (<i>n</i> = 20)	61.7	69.5
	Black women (<i>n</i> = 20)	65	68.8
	White men (<i>n</i> = 20)	66.1	69.5
	White women (<i>n</i> = 17)	64.9	67.7
Posterior to third molar	Black men (<i>n</i> = 20)	17.1	11.8
	Black women (<i>n</i> = 20)	18.2	12.9
	White men (<i>n</i> = 20)	16.2	11.4
	White women (<i>n</i> = 17)	18.7	13.5

Table 4 GPF dimensions in previous studies

Study	A-P dimension Mean (mm)	L-M dimension Mean (mm)
Tomaszewska et al. (2014) (3)	5.1	3.0
Nimigeen et al. (2013) (14)	4.9	3.0
Piagkou et al. (2012) (15)	5.3	2.7
Hwang et al. (2011) (19)	4.5	2.2
Klosek and Rungruang (2009) (2)	5.0	2.7
Methathrathip et al. (2005) (13)	4.9	2.7
Sharma and Garud (2013) (16)	4.7	3.3
Fu et al. (2011) (6)	4.6	2.8

molar association (73.45%) was also found in a Brazilian population (1,5); 22% of GPFs were distal to the third molars. Indian studies (13,17,18) reported GPFs close to third molars in 69.7% of cases and distal to third molars in 7.3% of cases. Our data showed that GPFs were close to the third maxillary molar in 66.65% of cases, which is consistent with findings from African and Indian studies. However, 14.98% of GPFs were distal to the third molar and 18.38% were anterior to it. Past and present findings indicate that GPF location varies in relation to population. However, this discrepancy might be attributable to the different classification systems used to identify GPF location in relation to maxillary molar teeth. We found that GPF location varied from the first maxillary molar to distal of the third molar in a South African population. Although some specimens had no maxillary molar teeth, GPF location could be accurately determined by using the average mesiodistal dimensions of premolar and molar teeth, as shown in our study.

The distance between the GPF and maxillary molar teeth is believed to be important, especially when harvesting soft tissue from the palate. A literature search

showed no conventional CT or CBCT study of these measurements. However, two cadaver studies reported results that might be relevant to our findings. In a study by Fu et al. (6) the average distance from the GPF to the cemento-enamel junction of the second and third molar teeth was 14.5 ± 2.4 mm. Another cadaver study, by Klosek and Rungruang (2), obtained vertical measurements from the alveolar crest of the second and third molars to the deepest point of the greater palatine sulcus: the average was 7.3 ± 2.9 mm. In our study the average distance from the GPF to the MP was 12.75 ± 3 mm, which is slightly shorter than the distance reported by Fu et al. (6). This discrepancy is explained by the fact that the cemento-enamel junction was used in their study and the alveolar crest was used in the present study. A study by Klosek and Rungruang (2) reported smaller average dimensions than those of Fu et al. (6) and the present study, perhaps because of differences in the populations studied (Thai, American, South African), sample size, and methods used. It should be noted that these cadaver studies used calipers to measure to the nearest millimeter. In our study the advanced volume rendering software

allowed measurements to the second decimal place. The use of cadaver dissection for analysis of anatomical structures is more challenging than analysis of a 3-D model with dedicated software.

Previous studies of GPF dimensions reported a mean A-P of 4.5 to 5.3 mm (16,19) and a mean L-M of 2.2 to 3.3 mm (17,19). Despite differences in the methods used to assess GPF, GPF dimensions did not significantly differ among studies (Table 4). The mean GPF dimensions in our study were an A-P of 5.22 mm and an L-M of 2.81 mm, which are consistent with previous findings. Although GPF location varies greatly by population, the GPF was adjacent or posterior to the third maxillary molar in 83.53% of our sample of South Africans. We used a new method to identify GPF position by calculating the average mesiodistal dimensions of premolar and molar teeth in skulls with no maxillary molars. Appropriate planning is necessary before performing surgical procedures involving this anatomical region. We recommend 3-D imaging for this purpose. Our findings should help clinicians understand and assess the anatomy of this region by using conventional imaging techniques.

Acknowledgments

We are grateful to Clarisa Sutherland for assistance with skull scanning.

Conflict of interest

The authors have no conflict of interest to declare.

References

- Ikuta CR, Cardoso CL, Ferreira-Junior O, Lauris JR, Souza PH, Rubira-Bullen IR (2013) Position of the greater palatine foramen: an anatomical study through cone beam computed tomography images. *Surg Radiol Anat* 35, 837-842.
- Klosek SK, Rungruang T (2009) Anatomical study of the greater palatine artery and related structures of the palatal vault: considerations for palate as the subepithelial connective tissue graft donor site. *Surg Radiol Anat* 31, 245-250.
- Tomaszewska IM, Tomaszewski KA, Kmiotek EK, Pena IZ, Urbanik A, Nowakowski M et al. (2014) Anatomical landmarks for the localization of the greater palatine foramen--a study of 1200 head CTs, 150 dry skulls, systematic review of literature and meta-analysis. *J Anat* 225, 419-435.
- Langenegger JJ, Lownie JF, Cleaton-Jones PE (1983) The relationship of the greater palatine foramen to the molar teeth and pterygoid hamulus in human skulls. *J Dent* 11, 249-256.
- Chrcanovic BR, Custodio AL (2010) Anatomical variation in the position of the greater palatine foramen. *J Oral Sci* 52, 109-113.
- Fu JH, Hasso DG, Yeh CY, Leong DJ, Chan HL, Wang HL (2011) The accuracy of identifying the greater palatine neurovascular bundle: a cadaver study. *J Periodontol* 82, 1000-1006.
- Rodella LF, Buffoli B, Labanca M, Rezzani R (2012) A review of the mandibular and maxillary nerve supplies and their clinical relevance. *Arch Oral Biol* 57, 323-334.
- Chen CC, Chen ZX, Yang XD, Zheng JW, Li ZP, Huang F et al. (2010) Comparative research of the thin transverse sectional anatomy and the multislice spiral CT on pterygopalatine fossa. *Turk Neurosurg* 20, 151-158.
- Rapado-Gonzalez O, Suarez-Quintanilla JA, Otero-Cepeda XL, Fernandez-Alonso A, Suarez-Cunqueiro MM (2015) Morphometric study of the greater palatine canal: cone-beam computed tomography. *Surg Radiol Anat* 37, 1217-1224.
- Hassanali J, Mwaniki D (1984) Palatal analysis and osteology of the hard palate of the Kenyan African skulls. *Anat Rec* 209, 273-280.
- Matsuda Y (1927) Location of the dental foramina in human skulls from statistical observations. *International Journal of Orthodontia, Oral Surgery and Radiography* 13, 299-305.
- Ajmani ML (1994) Anatomical variation in position of the greater palatine foramen in the adult human skull. *J Anat* 184 (Pt 3), 635-637.
- Methathathip D, Apinhasmit W, Chompoopong S, Lertsirithong A, Ariyawatkul T, Sangvichien S (2005) Anatomy of greater palatine foramen and canal and pterygopalatine fossa in Thais: considerations for maxillary nerve block. *Surg Radiol Anat* 27, 511-516.
- Nimigeau V, Nimigeau VR, Butincu L, Salavastru DI, Podoleanu L (2013) Anatomical and clinical considerations regarding the greater palatine foramen. *Rom J Morphol Embryol* 54, 779-783.
- Piagkou M, Xanthos T, Anagnostopoulou S, Demesticha T, Kotsiomitis E, Piagkos G et al. (2012) Anatomical variation and morphology in the position of the palatine foramina in adult human skulls from Greece. *J Craniomaxillofac Surg* 40, e206-210.
- Sharma NA, Garud RS (2013) Greater palatine foramen--key to successful hemimaxillary anaesthesia: a morphometric study and report of a rare aberration. *Singapore Med J* 54, 152-159.
- Jaffar AA, Hamadah HJ (2003) An analysis of the position of the greater palatine foramen. *J Basic Med Sci* 3, 24-32.
- Kumar A, Sharma A, Singh P (2011) Assessment of the relative location of greater palatine foramen in adult Indian skulls: consideration for maxillary nerve block. *Eur J Anat* 15, 150-154.
- Hwang SH, Seo JH, Joo YH, Kim BG, Cho JH, Kang JM (2011) An anatomic study using three-dimensional reconstruction for pterygopalatine fossa infiltration via the greater palatine canal. *Clin Anat* 24, 576-582.
- Tomaszewska IM, Kmiotek EK, Pena IZ, Sredniawa M, Czyzowska K, Chrzan R et al. (2015) Computed tomography morphometric analysis of the greater palatine canal: a study of 1,500 head CT scans and a systematic review of literature. *Anat Sci Int* 90, 287-297.